JOURNAL OF VIROLOGY, Aug. 2009, p. 7411–7421 Vol. 83, No. 15
0022-538X/09/$08.00+0 doi:10.1128/JVI.00079-09


# Characterization of a Highly Conserved Domain within the Severe Acute Respiratory Syndrome Coronavirus Spike Protein S2 Domain with Characteristics of a Viral Fusion Peptide[▽]

Ikenna G. Madu, Shoshannah L. Roth, Sandrine Belouzard, and Gary R. Whittaker*

*Department of Microbiology and Immunology, College of Veterinary Medicine, Cornell University, Ithaca, New York 14853*

Received 13 January 2009/Accepted 6 May 2009

**Many viral fusion proteins are primed by proteolytic cleavage near their fusion peptides. While the coronavirus (CoV) spike (S) protein is known to be cleaved at the S1/S2 boundary, this cleavage site is not closely linked to a fusion peptide. However, a second cleavage site has been identified in the severe acute respiratory syndrome CoV (SARS-CoV) S2 domain (R797). Here, we investigated whether this internal cleavage of S2 exposes a viral fusion peptide. We show that the residues immediately C-terminal to the SARS-CoV S2 cleavage site SFIEDLLFNKVTLADAGF are very highly conserved across all CoVs. Mutagenesis studies of these residues in SARS-CoV S, followed by cell-cell fusion and pseudotyped virion infectivity assays, showed a critical role for residues L803, L804, and F805 in membrane fusion. Mutation of the most N-terminal residue (S798) had little or no effect on membrane fusion. Biochemical analyses of synthetic peptides corresponding to the proposed S2 fusion peptide also showed an important role for this region in membrane fusion and indicated the presence of α-helical structure. We propose that proteolytic cleavage within S2 exposes a novel internal fusion peptide for SARS-CoV S, which may be conserved across the *Coronaviridae*.**

The severe acute respiratory syndrome coronavirus (SARS-CoV) emerged in 2003 as a significant threat to human health, and CoVs still represent a leading source of novel viruses for emergence into the human population. The CoV spike (S) protein mediates both receptor binding (via the S1 domain) and membrane fusion (via the S2 domain) and shows many features of a class I fusion protein, including the presence of distinct heptad repeats within the fusion domain (37). A critical feature of any viral fusion protein is the so-called "fusion peptide," which is a relatively apolar region of 15 to 25 amino acids that interacts with membranes and drives the fusion reaction (9, 34, 38). Fusion peptides can be classified as N-terminal or internal, depending on their location relative to the cleavage site of the virus fusion protein (23). One key feature of viral fusion peptides is that within a particular virus family, there is high conservation of amino acid residues; however, there is little similarity between fusion peptides of different virus families (26). Despite these differences, some common themes do emerge, including a high level of glycine and/or alanine residues, as well as critical bulky hydrophobic amino acids. In several cases, the fusion peptide is known to contain a central "kink." In the case of influenza virus hemagglutinin (HA), which is a classic example of an N-terminal fusion peptide, the N- and C-terminal parts of the fusion peptide (which are α-helical) penetrate the outer leaflet of the target membrane, with the kink at the phospholipid surface. The inside of the kink contains hydrophobic amino acids, with charged residues on the outer face (18). Internal fusion peptides (such as Ebola virus [EBOV] GP) often contain a conserved proline near their centers but also require a mixture of hydrophobic and flexible residues similar to N-terminal fusion peptides (9, 11). It is believed that the kinked fusion peptide sits in the outer leaflet of the target membrane and possibly induces positive curvature to drive the fusion reaction (22). It is important to note that, despite the presence of key hydrophobic residues, viral fusion peptides often do not display extensive stretches of hydrophobicity and can contain one or more charged residues (8). Ultimately, fusion peptide identification must rely on an often complex set of criteria, including structures of the fusion protein in different conformations, biophysical measurements of peptide function in model membranes, and biological activity in the context of virus particles.

To date, the exact location and sequence of the CoV fusion peptide are not known (4); however, by analogy with other class I viral fusion proteins, it is predicted to be in the S2 domain. Overall, three membranotropic regions in SARS-CoV S2 have been suggested as potential fusion peptides (14, 17). Based on sequence analysis and a hydrophobicity analysis of the S protein using the Wimley-White (WW) interfacial hydrophobic interface scale, initial indications were that the SARS-CoV fusion peptide resided in the N-terminal part of HR1 (heptad repeat 1) (5, 6), which is conserved across the *Coronaviridae*. Mutagenesis of this predicted fusion peptide inhibited fusion in syncytia assays of S-expressing cells (28). This region of SARS-CoV has also been analyzed by other groups in biochemical assays (16, 17, 29) and defined as the WW II region although Sainz et al. (29) actually identified another, less conserved and less hydrophobic, region (WW I) as being more important for fusion. Peptides corresponding to this region have also been studied in biochemical assays by other groups (13). In addition, a third, aromatic region adjacent to the transmembrane domain (the membrane-proximal domain) has been shown to be important in SARS-CoV fusion

* Corresponding author. Mailing address: Department of Microbiology and Immunology, Veterinary Medical Center, C4127, Cornell University, Ithaca NY 14853. Phone: (607) 253-4019. Fax: (607) 253-3385. E-mail: grw7@cornell.edu.

▽ Published ahead of print on 13 May 2009.

(15, 20, 25, 30). This membrane-proximal domain likely acts in concert with a fusion peptide in the S2 ectodomain to mediate final bilayer fusion once conformational changes have exposed the fusion peptide in the ectodomain. To date, there is little or no information on the fusion peptides of CoVs other than SARS-CoV, except for the identification of the N-terminal part of the mouse hepatitis virus (MHV) S HR1 domain as a putative fusion peptide based on sequence analysis (6). In none of these cases (for SARS-CoV or MHV) is the role of these sequences as bone fide fusion peptides established.

The majority of class I fusion proteins prime fusion activation by proteolytic processing, with the cleavage event occurring immediately N-terminal to the fusion peptide (21). In the case of SARS-CoV, early reports analyzing heterologously expressed SARS-CoV spike protein indicated that most of the protein was not cleaved (31, 39) but that there was some possibility of limited cleavage at the S1-S2 boundary (39). However, it is generally considered that S1-S2 cleavage is not directly linked to fusion peptide exposure in the case of SARS-CoV or any other CoV (4). Recently, however, it has been shown that SARS-CoV S can be proteolytically cleaved at a downstream position in S2, at residue 797 (2, 36). Here, we investigated whether cleavage at this internal position in S2 might expose a domain with properties of a viral fusion peptide. We carried out a mutagenesis study of SARS-CoV S residues 798 to 815 using cell-cell fusion and pseudovirus assays, as well as lipid mixing and structural studies of an isolated peptide, and we show the importance of this region as a novel fusion peptide for SARS-CoV.

## MATERIALS AND METHODS

**Cell culture.** BHK-21, Vero E6, and 293T cells obtained from the American Type Culture Collection were used in this study. All cells were maintained in Dulbecco's modified Eagle's medium (DMEM; Cellgro) containing 10% fetal bovine serum, 100 units/ml penicillin, and 10 μg/ml streptomycin (complete DMEM).

**Generation of mutant SARS-CoV spike glycoproteins.** Site-directed mutagenesis was carried out on the spike protein expressing vector pcDNA3.1-SARS-CoV S (kindly provided by Michael Farzan, New England Primate Research Center) via PCR, using primers obtained from IDT Technologies. Mutations were then confirmed by sequencing using an Applied Biosystems Automated 3730 DNA Analyzer at the Cornell University Life Sciences Core Laboratories Center.

**Analysis of SARS-CoV S cell surface expression.** BHK-21 cells were grown on six-well plates and transfected with 1 μg of wild-type or mutant spike protein-expressing plasmids using Lipofectamine 2000 (Invitrogen) for 36 h at 32°C. Transfected cells were washed twice with cold phosphate-buffered saline and then labeled with 250 μg/ml sulfo-NHS-SS-biotin [sulfosuccinimidyl 2-(biotinamido)-ethyl-1,3-dithiopropionate; Pierce] for 30 min on ice. Cold glycine solution (50 mM) was added to the cells three times at 5-min intervals to quench unlabeled free biotin, followed by a phosphate-buffered saline wash. The cells were lysed in 500 μl of lysis buffer (Tris-buffered saline containing 1% NP-40 and complete protease inhibitor mixture; Roche Applied Science). The lysates were affinity purified using immobilized NeutraAvidin beads (Pierce) overnight at 4°C. NeutraAvidin beads were then washed with lysis buffer, followed by the addition of sodium dodecyl sulfate-polyacrylamide gel electrophoresis (SDS-PAGE) sample loading buffer containing 100 mM dithiothreitol. The surface expression was analyzed by Western blotting using the anti-C9 epitope tag monoclonal antibody Rho 1D4 (National Cell Culture Center, Minneapolis, MN), and images were obtained and quantified using an LAS-3000 Mini Fuji film imaging system and software (Fuji Photo Film Co., Ltd). The biotinylation assay was repeated three times, and results from the Western blotting quantifications were plotted using Sigma Plot, version 9.0 (Systat Software).

**Syncytia formation and visualization.** BHK-21 cells in 24-well plates were cotransfected with pcDNA3.1-SARS-CoV S plasmid encoding wild-type or mutant spike protein and a plasmid encoding ACE2, the SARS-CoV receptor, using Lipofectamine 2000 (Invitrogen) for 24 h at 32°C. Cells were treated with 2 μg/ml of trypsin in serum free medium for 30 min to induce syncytia formation, and then the medium was replaced with complete DMEM for 1 h. The cells were then fixed using 3% paraformaldehyde and prepared for indirect immunofluorescence microscopy using the monoclonal SARS-CoV S antibody 341CD (NIH Biodefense and Emerging Infections Research Resources Repository) and Alexa Fluor 488-labeled anti-mouse secondary antibody (Invitrogen-Molecular Probes). Images were captured using a Nikon E600 microscope 20× Plan Apo objective (numerical aperture, 0.75) equipped with a SensiCam EM camera (Cooke Corp.) and using IP Lab software (Scanalytics).

**Quantitative cell-cell fusion assay.** BHK-21 cells were grown in 24-well plates and cotransfected with wild-type or mutant spike protein-expressing plasmids and a plasmid encoding luciferase under the control of a T7 promoter, using Lipofectamine 2000 (Invitrogen) for 24 h at 32°C. Vero E6 cells in a 60-mm dish were also transfected with a plasmid encoding the T7 polymerase. After 24 h the BHK-21 cells were overlaid with Vero E6 cells and incubated for 3 h. Cells were treated with serum-free medium containing 2 μg/ml trypsin to induce fusion, which was replaced with complete DMEM after 30 min. At 6 h postinduction, cells were lysed and assayed for luciferase activity using a luciferase assay kit (Promega) and a Glomax 20/20 luminometer (Promega) to measure light emission.

**Spike protein pseudotyped virion production.** Pseudotyped virions were generated using plasmids kindly provided by Jean Dubuisson (Lille Pasteur Institute, France). 293T cells were cotransfected with a murine leukemia virus (MLV)-based transfer vector encoding luciferase, an MLV Gag-Pol packaging construct, and pcDNA3.1-SARS-CoV S, a plasmid encoding wild-type or mutant spike envelope glycoprotein, using Exgen 500 (Fermentas) as recommended. After incubation for 72 h at 32°C, supernatants were collected and filtered through a 0.45-μm-pore-size membrane. The level of spike protein incorporation was confirmed by polyethylene glycol (PEG) concentration, centrifugation, and Western blot analysis. A total of 600 μl of filtered supernatant was mixed with 200 μl of 40% PEG and centrifuged for 30 min at 4,000 rpm at 4°C. The pellet was redissolved in SDS-PAGE sample loading buffer containing 100 mM dithiothreitol and blotted in the same manner as described above in the cell surface biotinylation assay.

**Spike protein pseudotyped virion infectivity assays.** Equal levels of pseudoparticles were used based on the level of spike protein pseudotype virions quantified by Western blotting, as described above. For a typical infection assay, spike protein pseudotype virions containing wild-type or mutant glycoproteins were bound for 2 h in RPMI medium containing 0.2% bovine serum albumin (BSA)–20 mM HEPES to Vero E6 cells at 4°C. Medium was exchanged for complete DMEM and incubated for 48 h at 37°C. The cells were then lysed, and luciferase activity was measured using the same methods as the quantitative cell-cell fusion assay. In a trypsin-mediated cell surface infectivity assay, Vero E6 cells were first preincubated with 25 mM $NH_4Cl$ for 1 h at 37°C. Pseudotyped virions were then bound for 2 h in RPMI medium containing 0.2% BSA, 20 mM HEPES, and 25 mM $NH_4Cl$ at 4°C. The cells were then warmed up with the addition of prewarmed RPMI medium containing 5 μg/ml trypsin, 0.2% BSA, 20 mM HEPES, and 25 mM ammonium chloride for 5 min at 37°C in a water bath.

**Peptides.** The SARS-CoV S2 fusion peptides SFIEDLLFNKVTLADAGFM KQYGCGKKKK, SFIEDLLFGCGKKKK, and SFIEDAAAGCGKKKK were synthesized using solid-phase techniques by New England Peptide (Gardner, MA). The GCGKKKK linker was included to promote liposome association as described for the host-guest fusion peptide system of Han et al. (19). Purity as determined by high-performance liquid chromatography was greater than 95%, and mass identification was performed by matrix-assisted laser desorption ionization–time of flight mass spectrometry. Peptides were resuspended to 5 mg/ml sterile MilliQ water. Control peptides were treated identically and had the sequence SIRYSFCGNGRHV for circular dichroism (CD) spectroscopy experiments and GCGKKKK for lipid-mixing experiments.

**Liposomes.** 1-Palmitoyl-2-oleoyl-*sn*-glycero-3-phosphocholine (POPC), 1-palmitoyl-2-oleoyl-*sn*-glycero-3-[phospho-L-serine] (sodium salt) (POPS), and cholesterol were purchased from Avanti Polar Lipids (Alabaster, AL). Labeled phospholipids *N*-(7-nitrobenz-2-oxa-1,3-diazol-4-yl)-1,2-dihexadecanoyl-*sn*-glycero-3-phosphoethanolamine, triethylammonium salt (NBD-PE) and lissamine rhodamine B 1,2-dihexadecanoyl-*sn*-glycero-3-phosphoethanolamine, triethylammonium salt (Rho-PE) were purchased from Invitrogen (Carlsbad, California). Large unilamellar vesicles were prepared according to the extrusion method. Lipid films were obtained by subjecting chloroform-dissolved lipid mixtures at a ratio of 1:3:1 of POPC-POPS-cholesterol to high vacuum overnight. Lipid films were resuspended by the addition of fusion buffer (5 mM HEPES, 5 mM morpholinethanesulfonic acid, 5 mM sodium succinate, 150 mM sodium chloride, pH 7) to a 5 or 10 mM lipid concentration and incubated for 15 min at room temperature, followed by vortexing for 15 min.

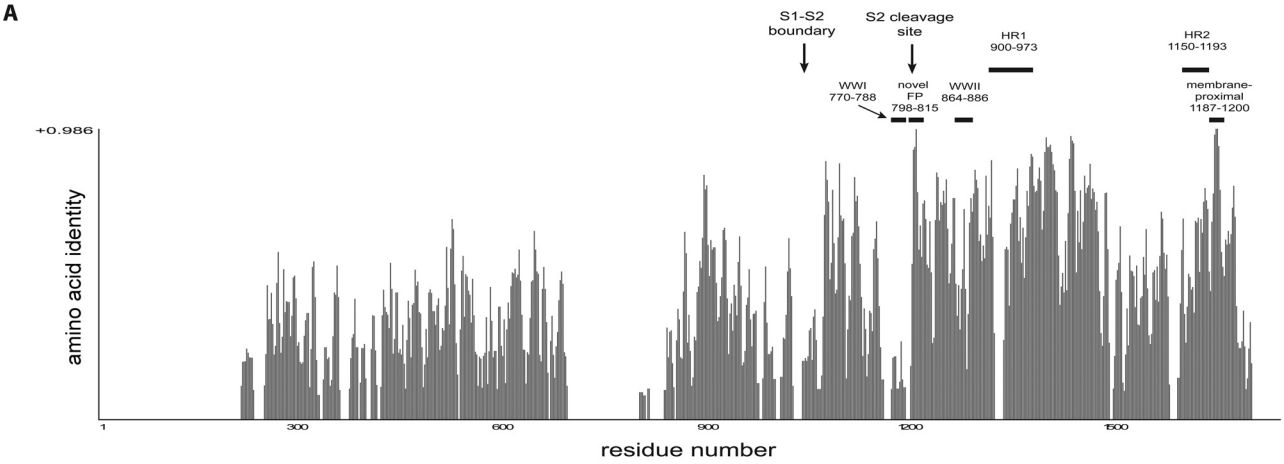


B

| | | | | | |
|---|---|---|---|---|---|
| Group 2 | SARS-CoV (TOR2) | SFIEDLLFNKVTLADAG-F 815 | Group 1 | HCoV-NL63 (Amsterdam) | SALEDLLFSKVVTSGLGTV 889 |
| | Sable Antelope CoV (US/OH1/03) | SAIEDLLFSKVKLSDVG-F 931 | | HCoV-229E | SAIEDILFSKLVTSGLGTV 708 |
| | Giraffe CoV (US/OH3-TC/2006) | SAIEDLLFSKVKLSDVG-F 926 | | PEDV (LZC) | SVIEDLLFNKVVTNGLGTV 910 |
| | Bovine CoV (R-AH187) | SAIEDLLFSKVKLSDVG-F 931 | | FIPV (79-1146) | SAIEDLLFDKVVTSGLGTV 980 |
| | HCoV-OC43 (ATCC VR-759) | SAIEDLLFDKVKLSDVG-F 929 | | TGEV (Pur476-MAD) | SAIEDLLFDKVVTSGLGTV 977 |
| | PHEV (VW572) | SAIEDLLFDKVKLSDVG-F 917 | | PRCoV (ISU-1) | SAIEDLLFSKVVTSGLGTV 750 |
| | Equine CoV (NC99) | SAIEDLLFNKVRLSDVG-F 931 | | Bat CoV (BTCov/273/05) | SFIEDLLYNKVTLADAG-F 801 |
| | HCoV-HKU1 (N19) | SFFEDLLFDKVKLSDVG-F 922 | | | |
| | MHV (A59) | SAIEDLLFDKVKLSDVG-F 887 | Group 3 | IBV (M41) | SFIEDLLFFTSVESVGLP- 708 |
| | MHV-2 | SAIEDVLFDKVKLSDVG-F 925 | | IBV (Bdtte) | SVIEDLLFTSVESVGLP-T 708 |

FIG. 1. Bioinformatics analysis of the CoV S protein and the proposed S2 fusion peptide. (A) A quantitative multiple sequence alignment of the S protein from representative CoVs was performed using the program AlignX, a component of Vector NTI 10.3.1 (Invitrogen), which uses a modified Clustal W algorithm. The proposed S2 fusion peptide and other regions of interest have been identified with bars or arrows to show their location within the S gene and their various degrees of conservation across the CoV family. (B) A multiple sequence alignment of the S protein from representative CoVs was performed using AlignX as above. Conserved residues within the proposed S2 fusion peptide region are indicated in bold. Underlining indicates residues showing conserved properties. Virus abbreviations (and GenBank accession numbers) are as follows: SARS-CoV (AAP13441); HCoV-NL63, human CoV NL63 (Amsterdam accession number AAS58177); HCoV-229E, human CoV 229E (AAG48592); HCoV-OC43, human CoV OC43 ATCC VR-759 (AAR01015); HCoV-HKU I, human CoV HKU I N19 (ABD75497); IBV (Bdtte), infectious bronchitis virus Beaudette strain (AAY24433); IBV (M41), infectious bronchitis virus M41 strain (ABI26423); MHV-A59, MHV A59 (AAB86819); MHV-2, MHV 2 (AAF19386); PEDV, porcine epidemic diarrhea virus LZC (ABM64776); PRCoV, porcine CoV ISU-1 (ABG89317); PHEV, porcine hemagglutinating encephalomyelitis virus VW752 (AAY68297); bovine CoV, bovine CoV R-AH187 (ABP38295); sable antelope CoV, sable antelope CoV US/OH1/2003 (ABP38306); giraffe CoV, giraffe CoV US/OH3-TC/2006 (ABP38313); equine CoV, equine CoV NC99 (ABP87990); FIPV, feline infectious peritonitis virus WSU 79-1146 (YP239355); bat CoV, bat CoV 273/2005 (ABG47069); TGEV, transmissible gastroenteritis virus Purdue PUR46-MAD (NP058424).

Liposomes were then subjected to 10 freeze-thaw cycles, followed by 11 cycles of extrusion through a 0.1-μm-pore-size polycarbonate membrane using an Avanti mini-extruder. Liposomes labeled with the fluorescent resonance energy transfer (FRET) pairs Rho-PE and NBD-PE were made in the same manner with the addition of 0.6% each of NBD-PE and Rho-PE to the chloroform-dissolved lipid mixture.

**Lipid-mixing assay.** Lipid mixing was determined using the method of Struck et al. (32). Unlabeled and labeled liposomes were mixed at a 4:1 ratio to a total concentration of 110 μM lipid in fusion buffer at pH 7.0. Hydrochloric acid was added to the solution until the desired pH was achieved. To initiate fusion, peptide was added to the specified concentration. To end the reaction and obtain a measurement of 100% lipid mixing, reduced Triton X-100 was added to a final concentration of 0.2%. Changes in fluorescence were measured using a QM-6SE spectrofluorimeter (Photon Technology International, Birmingham, NJ) with excitation set at 467 nm and emission monitored at 530 and 581 nm. The extent of lipid mixing was determined using the following formula: $F(\%) = [(f_t - f_0)/(f_{100} - f_0)] \times 100$, where $f_t$ is the fluorescence measurement at time $t$, $f_0$ is the initial fluorescence, and $f_{100}$ is the fluorescence after the addition of reduced Triton X-100. All measurements were taken in triplicate and averaged.

**CD spectroscopy.** Spectra were obtained using an Aviv Biomedical CD spectrometer, model 202-01, equipped with a thermoelectric temperature controller. Spectra were obtained at a 50 μM peptide concentration in 50% trifluoroethanol (TFE) at 37°C. A wavelength range of 190 to 260 nm and averaging time of 2 s were used. Alpha-helical content was calculated using the following formula: $f_H = (\theta_{222} - \theta_C)/(\theta_H - \theta_C)$, where $\theta_C$ is 2,220 −53T, $\theta_H$ is (250T − 44,000)(1 − 3/$n$), $T$ is the temperature in Celsius, and $n$ is the number of residues in the peptide.

## RESULTS

**Bioinformatics and mutational analysis of the proposed CoV fusion peptide.** Based on the internal S2 cleavage site of SARS-CoV at R797, a predicted fusion peptide exposed by such cleavage would start at residue serine 798 and extend to phenylalanine 815. One common feature of viral fusion peptides is that they show a high degree of conservation within a virus family (26). We therefore performed a multiple sequence alignment of the spike protein of representative CoVs. This bioinformatics analysis showed a very high degree of conservation in the site of the proposed S2 fusion peptide (residues 798 to 815) (Fig. 1A). Indeed, residues 798 to 815 represent some of the most conserved spike protein residues across the *Coronaviridae*. In particular, the domain IEDLLF shows >95% identity, with only limited and very conservative substitutions (I–L/F, L–I/V, and F–Y) in the core hydrophobic residues and with 100% conservation of the initial serine residue

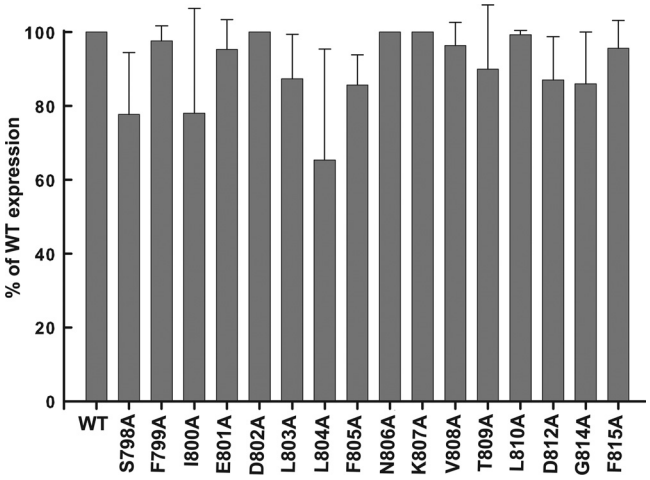


FIG. 2. Effect of alanine point mutants on spike protein surface expression. BHK cells were transfected with plasmids encoding wild-type SARS-CoV S or alanine mutants. The cells were labeled with sulfo-NHS-SS-biotin and lysed. Lysates were affinity purified with NeutraAvidin beads and resolved by SDS-PAGE and Western blotting using anti-S monoclonal antibody C9. The biotinylation assay was repeated three times, and the results from the Western blotting were quantified using IP Lab software and plotted in Sigma Plot, version 9.0. Error bars represent standard deviations of the means. WT, wild type.

(Fig. 1B). This highly conserved region is consistent with the requirements for a viral fusion peptide as it contains both small and bulky hydrophobic residues interspersed with more hydrophilic residues. While the juxtamembrane region is also highly conserved, the other proposed SARS-CoV S fusion peptides (WWI and WWII) show a much lower degree of conservation (Fig. 1B).

To test the fusogenic properties of the conserved S2 region (residues 798 to 815), mutations were introduced into a SARS-CoV S protein-expressing vector to generate the following mutants: S798A, F799A, I800A, E801A, D802A, L803A, L804A, F805A, N806A, K807A, V808A, T809A, L810A, D812A, G814A, and F815A (Fig. 1B). In order to evaluate the effect of point mutants on the fusogenic properties of SARS-CoV S protein, we first verified the cell surface expression of the mutants. The level of surface expression of the alanine point mutants was verified quantitatively after transfection of expression vectors bearing mutant or wild-type S protein in BHK-21 cells, at both 37°C and 32°C, followed by biotinylation and immunoblotting. At 37°C, we observed medium to low levels of surface expression of many of the mutants (data not shown), but at 32°C we were able to observe all mutants expressing at >65% of wild-type levels, and in most cases expression was >85% of wild-type levels (Fig. 2).

With high-level expression at the cell surface verified, we were then able to evaluate how the mutated residues might affect membrane fusion. Taking advantage of trypsin as a fusion trigger for the spike protein, we employed two methods of determining cell-cell fusion. The first method was a qualitative assessment of the mutant's ability to form syncytia in the presence of trypsin, which was performed by analyzing BHK-21 cells cotransfected with wild-type or mutant spike protein and ACE2, the SARS-CoV host cell receptor (Fig. 3). We observed a range of fusion events upon treatment with trypsin. In wild-type SARS-CoV S-expressing cells, trypsin treatment resulted in the production of large syncytia in comparison to nontreated cells expressing the spike protein. Mutation of the core conserved residues, i.e., I800A, L803A, L804A, F805A, K807A, and V808A, produced only limited fusion events in comparison to wild-type trypsin-treated cells, with the degree of syncytia comparable in some instances to wild-type levels in non-trypsin-treated cells. We also observed that the L810A, D812A, G814A, and F815A mutants in the C-terminal portion of the fusion peptide also displayed poor syncytia. In other alanine substitution mutants, i.e., S798A, D802A, N806A, and T809A, we saw similar levels of fusion in cells activated by trypsin and the wild-type protein.

In order to quantify the extent of the SARS S protein-mediated membrane fusion activity, a luciferase-based assay system was employed. In this assay, BHK-21 cells were cotransfected with wild-type or mutant spike protein along with a T7 polymerase-driven luciferase gene and overlaid with Vero E6 cells transfected with the T7 polymerase gene. Fusion was induced by trypsin treatment, and the degree of luciferase activity after induction of fusion was used as an indicator of the fusogenic ability of the mutant SARS-CoV S protein in comparison to the wild type (Fig. 4). We observed a variation of activity in response to mutation of the conserved S2 region (residues 798 to 815). Mutation of the core conserved residues, such as I800, L803, L804, F805, K807, V808, L810, D812, G814, and F815, resulted in luciferase activity that was 20% or less than wild-type activity, with the mutation at L804 producing activity close to background levels. Mutation of other residues, such as F799, E801, N806, and T809, showed 50% or less of wild-type activity. In contrast, mutations of residues S798 and D802 revealed no major differences from wild-type levels (fusion activity of >70%).

**Effects of SARS-CoV S fusion peptide mutants in MLV pseudotyped virions.** To better understand the roles of these fusion peptide residues in the context of a virus particle, we employed a retrovirus-based pseudovirion system (1). Based on the cell-cell fusion assays described above, we selected the core conserved residues identified as being critical to the fusion process as candidates for SARS-CoV S-expressing pseudoviral particles. In this infectivity assay, 293T cells were first cotransfected with an MLV Gag-Pol and luciferase plasmid along with either the SARS-CoV wild-type or mutant S protein plasmid or with an empty vector control to generate SARS-CoV S or control pseudotyped viral particles. The transfected cells were then incubated for 72 h at 32°C as this temperature was optimal for surface expression of the mutants. We first confirmed that a suitable level of expression of mutant spike protein was incorporated in the viral particles, in comparison to wild type, by blotting for spike protein in the collected supernatant 72 h posttransfection (Fig. 5A). With many of the mutants expressing at levels greater than 60% of the wild type, we observed a relative lack of spike protein incorporation in the S798A, I800A, E801A, L803A, and L804A mutants. The level of cell surface expression in 293T cells was also confirmed by our biotinylation assay (data not shown). In order to counter this lack of incorporation, we generated additional point mutants with the goal of identifying mutations that would allow efficient incorporation into pseudoparticles. We generated the following mutations: S798G, S798L, S798H, I800G, I800S, E801L,

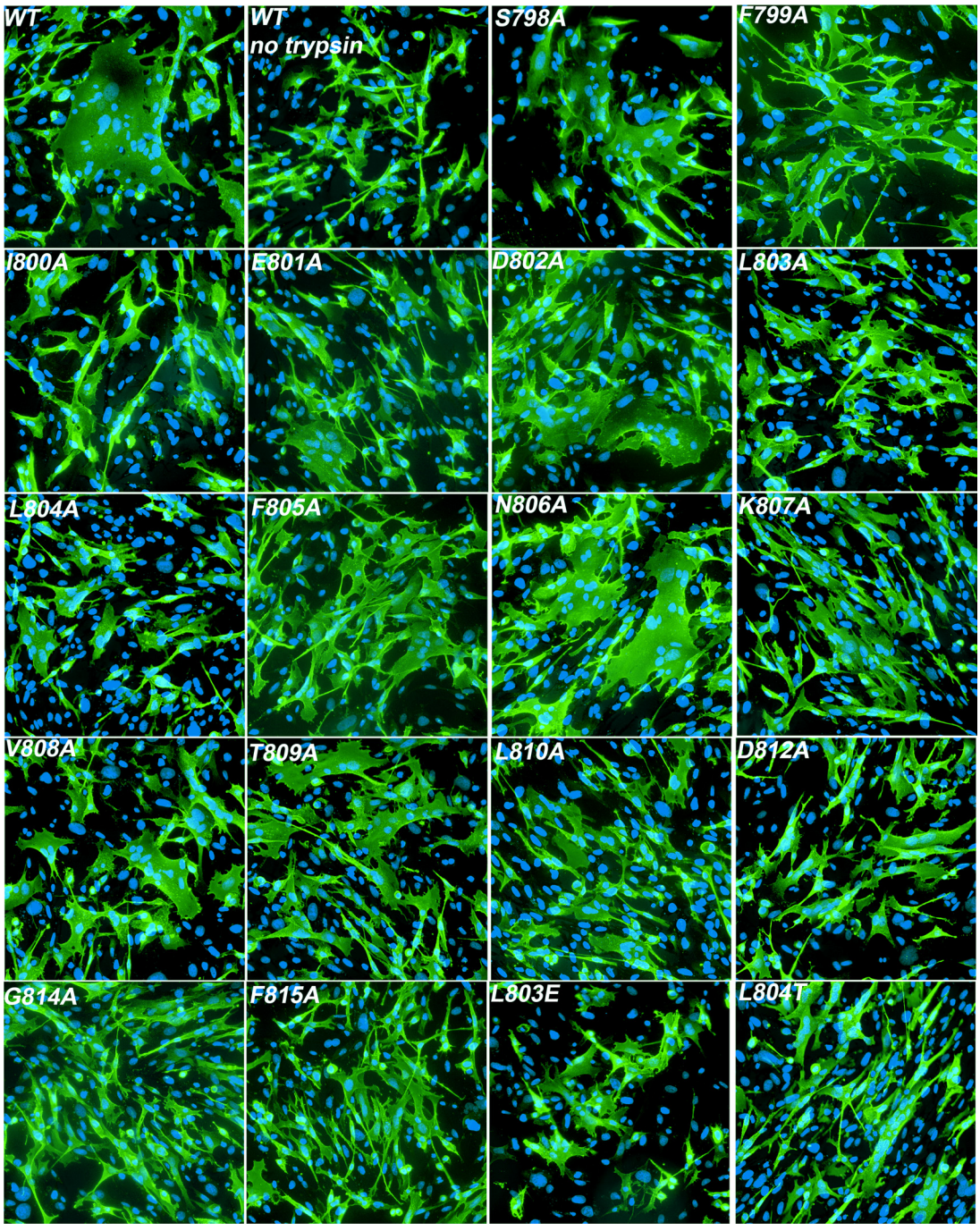


FIG. 3. Syncytium formation mediated by mutant spike proteins. BHK cells were transfected with plasmids encoding wild-type (WT) SARS-CoV S or alanine mutants and ACE2. Fusion was induced using medium containing 2 μg/ml trypsin as described in Materials and Methods, and syncytia were visualized by immunofluorescence microscopy using anti-S antibodies (green signal). Nuclei were counterstained with Hoechst 33264 (blue signal).

L803E, L803T, L804E, and L804T. All of these mutants were tested for the level of surface expression and incorporation into pseudotyped viral particles; however, only L803E and L804T (Fig. 5B) showed incorporation above 60% in comparison to the wild type.

Upon confirmation of mutant spike protein incorporation, Vero E6 cells were then transduced with SARS-CoV S pseudovirions, ensuring that equal amounts of viral particles were used in the infectivity assay by adjusting the volume of the supernatant. At 72 h posttransduction, cells were lysed, and luciferase activity was measured as an indicator of the extent of viral infection. The luciferase activity of the wild type was normalized to 100%, and luciferase activities of the mutants were compared to those of the wild type. As shown in Fig. 6A,

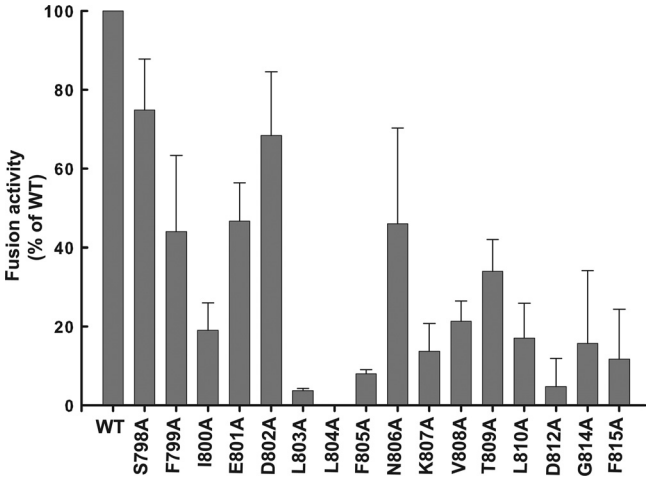


FIG. 4. Quantitative assays of membrane fusion mediated by mutant spike proteins. BHK cells were cotransfected with plasmids encoding wild-type (WT) SARS-CoV S or alanine mutants and also with luciferase cDNA under the control of a T7 promoter. At 24 h posttransfection, BHK cells were then overlaid with Vero cells previously transfected with a plasmid encoding T7 polymerase. After 3 h, fusion was induced using medium containing 2 μg/ml trypsin. The cells were lysed 6 h postfusion induction, and supernatants were measured for luciferase activity. Each bar is averaged from three individual repeats, and error bars represent standard deviations from the means.

we observed a distinct pattern that was similar to the quantitative cell-cell fusion data (Fig. 4). A marked reduction in infectivity in the core of the proposed fusion peptide, especially in mutants L803E, L804T, F805A, V808A, and L810A, was observed in the pseudovirus infectivity assay. We also observed

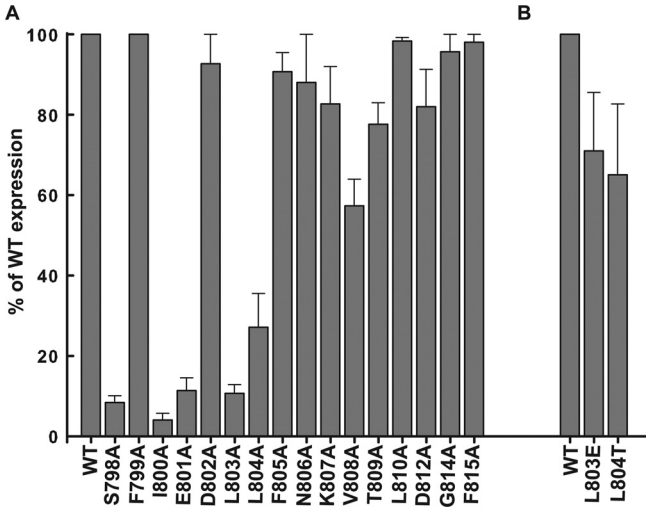


FIG. 5. Incorporation of mutant spike proteins into MLV pseudotyped virions. Spike protein-MLV pseudotyped virions were prepared as described in Materials and Methods. Virions were concentrated using a 10% PEG precipitation, diluted in SDS sample buffer, and resolved by SDS-PAGE and Western blotting using a monoclonal antibody specific for the C9 tag. The spike protein-MLV pseudotyped virions were generated three times for wild type (WT) or mutants, and the results from the Western blotting were quantified using IP Lab software and plotted in Sigma Plot, version 9.0. Error bars represent standard deviations from the means.

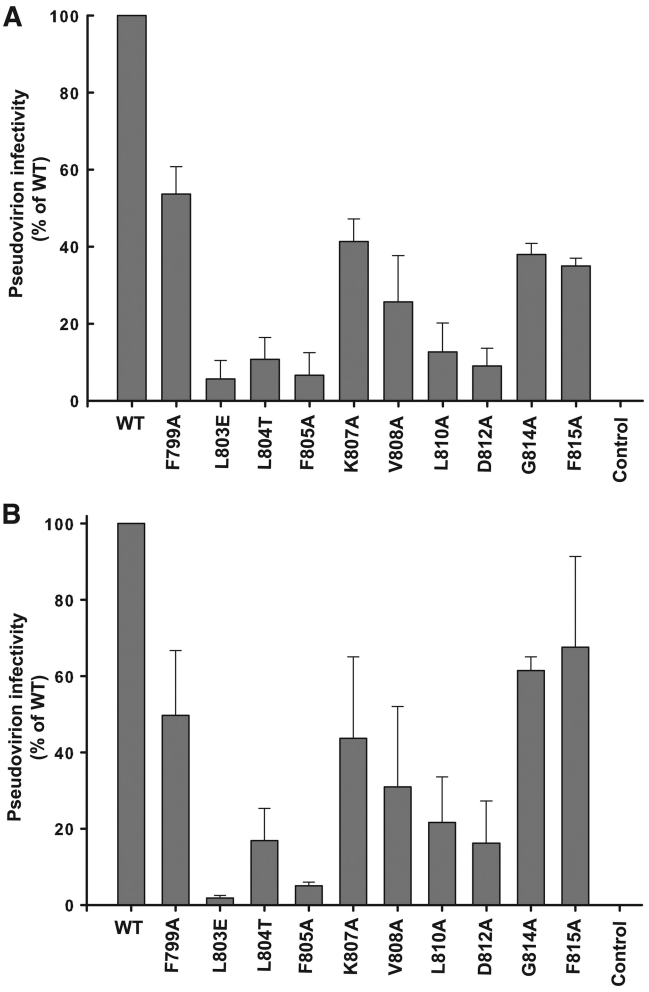


FIG. 6. Infectivity of spike protein-MLV pseudotyped virions. (A) Endosomal infectivity of spike protein-MLV pseudotyped virions. Virions were bound to Vero cells at 4°C in RPMI medium for 2 h. After binding, cells were rinsed in RPMI medium; the medium was then replaced with complete DMEM, and cells were incubated at 37°C. At 48 h postbinding cells were lysed and assayed for luciferase activity. (B) Trypsin-mediated infectivity of spike protein-MLV pseudotyped virions. Virions were bound to Vero cells at 4°C in RPMI medium and treated with 25 mM ammonium chloride. Fusion was induced using serum-free medium containing 2 μg/ml trypsin. The cells were lysed at 48 h postfusion induction, and supernatants were assayed for luciferase activity. Each bar is averaged from three individual infectivity assays, and error bars represent standard deviations of the means. WT, wild type.

that the mutation of residues flanking the core, such as F799A, K807A, G814A, and F815A, have less effect in virus entry assays than suggested by the corresponding cell-cell fusion data.

It is considered that SARS-CoV has the ability to fuse in both endocytic and nonendocytic compartments, and so we assessed any potential differences in the role of the proposed fusion peptide in each of these two pathways of virus entry. We therefore inhibited infection by the endocytic route using the lysosomotropic base $NH_4Cl$ and induced fusion of surface-bound virions by trypsin activation. At 48 h after trypsin treatment, cells were assayed for luciferase activity. We observed

| | | Cell-Cell fusion | Pseudotyped Virus infectivity | |
|---|---|---|---|---|
| | | | − trypsin | + trypsin |
| SARS WT | SFIEDLLFNKVTLADAGF | +++ | +++ | +++ |
| S798A | A---------- | ++ | ND | ND |
| F799A | -A--------- | + | ++ | + |
| I800A | --A-------- | − | ND | ND |
| E801A | ---A------- | + | ND | ND |
| D802A | ----A------ | ++ | +++ | +++ |
| L803A | -----A----- | − | ND | ND |
| L803E | -----E----- | ND | − | − |
| L804A | ------A---- | − | ND | ND |
| L804T | ------T---- | ND | − | − |
| F805A | -------A--- | − | − | − |
| K807A | ---------A- | − | + | + |
| V808A | ----------A | + | + | + |
| T809A | ----------A- | + | +++ | +++ |
| L810A | ----------A- | − | − | + |
| D812A | ----------A- | − | − | − |
| G814A | ----------A- | − | + | ++ |
| F815A | ----------A | − | + | ++ |

FIG. 7. Summary of effects of S2 mutations on SARS-CoV S fusion activity. The fusion activity of SARS-CoV S wild-type (WT) and mutants in cell-cell fusion assays, as well as in pseudovirus assays of endosomal (− trypsin) and nonendosomal (+ trypsin) infection are summarized. +++, 80 to 100% of wild-type level; ++, 79 to 50% of wild-type level; +, 49 to 20% of wild-type level; and −, <20% of wild-type level. ND, not determined.

that, with the exception of G814 and F815, almost all the residues highlighted in the trypsin-untreated assay as being important for infection were also critical in this assay of nonendosomal infection (Fig. 6B). These residues show responses that vary from about 50% for F799A down to almost background levels, as observed in L803E. Data for cell-cell fusion and pseudovirus assays are summarized in Fig. 7.

**Isolated peptides corresponding to the proposed SARS-CoV S2 fusion peptide promote lipid mixing.** In order to determine the ability of our proposed fusion peptide to mediate membrane fusion, we utilized a FRET-based assay of lipid mixing (32). In this assay, if a peptide is able to mediate lipid mixing, labeled and unlabeled liposomes fuse, resulting in a dilution of FRET pairs present in the labeled liposomes and an increase in fluorescence of the donor chromophore. The extent of lipid mixing mediated by the SARS S2 peptide (SFIEDLLFNKVT LADAGFMKQYGCGKKKK) and a negative control are shown in Fig. 8A. Lipid mixing was investigated at several concentrations of peptide, as well as at both pH 5 and pH 7. The SARS-CoV S2 peptide promoted a greater extent of lipid mixing at a lower pH. At higher concentrations of peptide, lipid mixing was also evident at pH 7. The negative control peptide showed no lipid mixing at any concentration or pH tested. The extent of lipid mixing of the SARS-CoV S2 peptide as a function of pH is shown in Fig. 8B. We also tested a shorter version of the peptide (SFIEDLLFGCGKKKK), which also showed efficient lipid mixing (Fig. 8C and D). The short peptide was also somewhat dependent on pH, but the effects of low pH were less pronounced than with the longer peptide. To examine the function of SARS-CoV S residues L803, L804, and F805 in the context of isolated peptides, we tested a modified short peptide (SFIEDAAAGCGKKKK). In contrast to wild-type sequence, the modified LLF-AAA peptide showed no ability to induce lipid mixing.

**CD spectroscopy indicates that the proposed SARS-CoV S2 fusion peptide has a helical secondary structure.** With fusion peptides of many other class I fusion proteins, e.g., influenza virus HA, characterized to be predominantly alpha-helical in secondary structure, we were interested in the structure of the SARS-CoV S2 peptide and used CD spectroscopy as a way to resolve its secondary-structure content (Fig. 9). The structure of the synthetic peptide SFIEDLLFNKVTLADAGFMKQYG CGKKKK was resolved in the presence and absence of TFE. TFE is a solvent used in many CD spectroscopy studies and functions to stabilize only structures that have the propensity to be helical (12). In the presence of TFE, the S2 fusion peptide gave a spectrum consistent with its having α-helical content; this was quantified to be approximately 37% α-helix. In the absence of TFE, the peptide maintained a structure in close resemblance to a random coil (Fig. 9A). A control peptide sequence downstream of the proposed S2 fusion peptide (residues 1021 to 1034) was used as a control. We also observed a major difference in the spectra of the proposed S2 fusion peptide compared to the control peptide, which maintained a structure closely resembling a random coil even in the presence of TFE (Fig. 9B). We also examined the structure of the shorter peptide SFIEDLLF. In the presence of TFE, the short S2 peptide also gave a spectrum consistent with its having a high degree of α-helical content, which was quantified to be approximately 77% α-helix (Fig. 9C).

## DISCUSSION

A common property of class I fusion proteins is that a proteolytic priming event is necessary for subsequent fusion activation that occurs following exposure to low pH and/or receptor binding. Proteolytic priming is classically associated with members of the trypsin or furin families (21), but more recently cathepsin family members have also been shown to prime fusion activation (38). In canonical class I fusion proteins, such as influenza virus HA or human immunodeficiency virus type 1 Env, proteolytic cleavage occurs directly N-terminal to the fusion peptide, in which case this is referred to as an "external," N-terminal fusion peptide (23, 38). In other cases, notably infection with avian leukosis sarcoma virus (ASLV) or EBOV, proteolytic priming still occurs with the cleavage site close to, but upstream from, the fusion peptide—in which case this is referred to as an "internal" fusion peptide (23, 38). Internal fusion peptides are generally considered to be relatively long (25 to 30 amino acids) and comprise an extended α-helix in the fusion-active state. In contrast, external class I fusion peptides are shorter (approximately 15 amino acids) and tend to have a helix-turn-helix structure, often with a central proline residue(s). In the case of CoV S proteins, proteolytic cleavage between the S1 and S2 domain often occurs, but there are no indications that this cleavage results in the exposure of a fusion peptide (4). Therefore, the S protein is generally considered to be a class I fusion protein with an internal fusion peptide.

Recently, it has become apparent that cleavage at a second position (R797) also occurs in the SARS-CoV protein (2, 36), and we hypothesized that this second cleavage event might expose a critical fusion peptide for the S protein. The sequence immediately C-terminal to the R797 cleavage site of SARS-CoV S is SFIEDLLFNKVTLADAGF, and we assessed this peptide as a potential viral fusion peptide. The first factor we considered with regard to the potential of this peptide as a

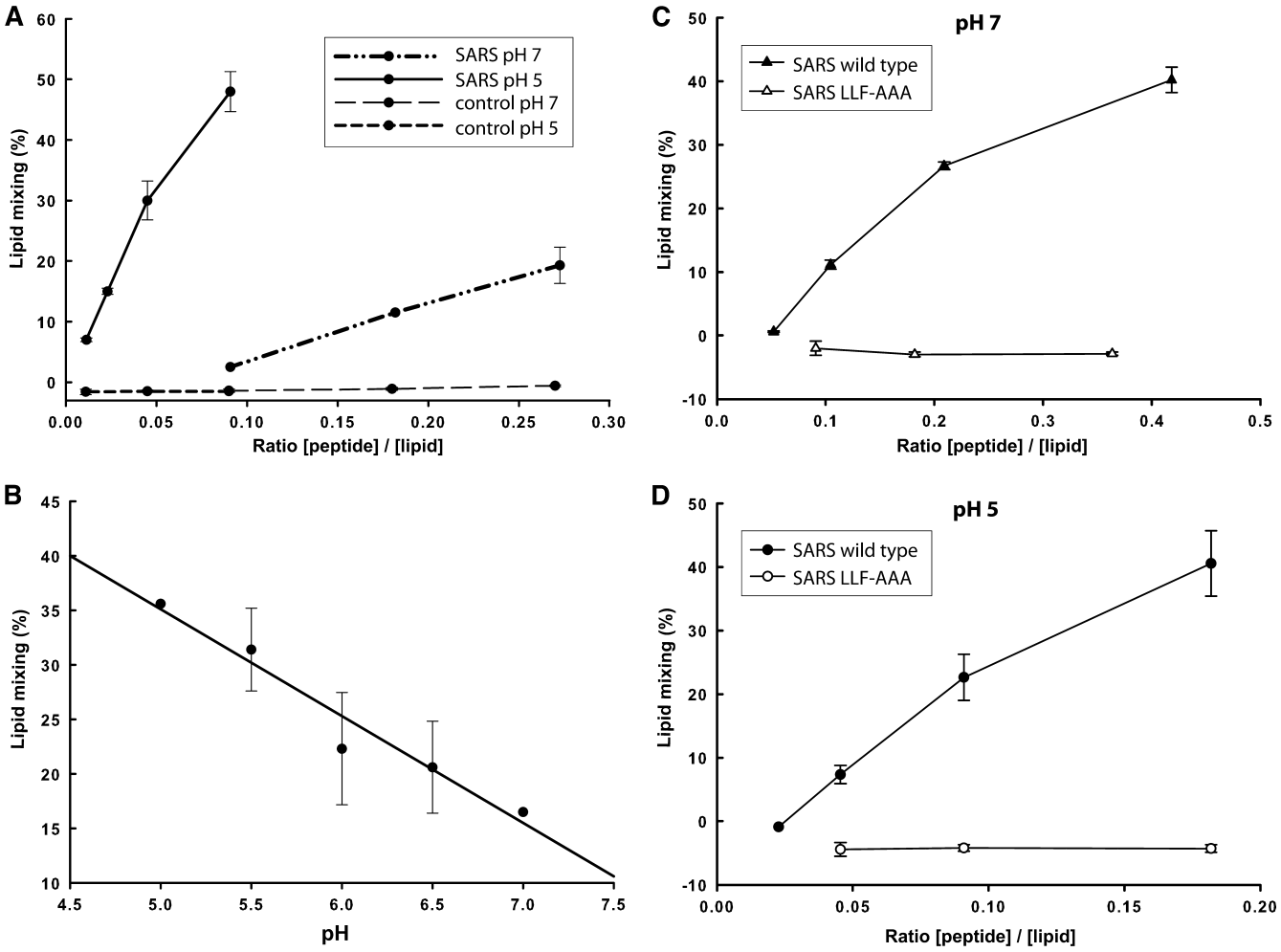


FIG. 8. The proposed SARS-CoV S2 fusion peptide induces lipid mixing in liposomes. (A) Extent of lipid mixing was determined by varying the ratios of SARS-CoV S2 fusion peptide or control peptide concentrations with the total concentration of labeled and unlabeled POPC-POPS-cholesterol (1:3:1) liposomes at pH 5 and pH 7. The kinetics of mixing was followed by monitoring fluorescence intensity at 530 nm upon addition of peptide. Each data point is averaged from three individual assays, and error bars represent standard deviations of the means. (B) Effect of SARS-CoV S2 fusion peptide on lipid mixing at various pH values. The kinetics of lipid mixing was followed by monitoring NBD-PE fluorescence intensity at 530 nm in decreasing-pH environments (from pH 7.0 to pH 4.5). Each data point is averaged from three individual assays, and error bars represent standard deviations of the means. (C) Extent of lipid mixing at pH 7 was determined by varying the ratios of wild-type or modified LLF-AAA SARS-CoV S2 fusion peptide with POPC-POPS-cholesterol (1:3:1) liposomes at various ratios of peptide to lipid. Each data point is averaged from three individual assays, and error bars represent standard deviations of the means. (D) Extent of lipid mixing at pH 5 was determined by varying the ratios of wild type or modified LLF-AAA SARS-CoV S2 fusion peptide with POPC-POPS-cholesterol (1:3:1) liposomes at various ratios of peptide to lipid. Each data point is averaged from three individual assays, and error bars represent standard deviations of the means.

bona fide fusion peptide was the degree of conservation across the *Coronaviridae*. As shown in Fig. 1, the peptide was extremely well conserved across all CoVs. In particular, the IE DLLF motif showed only minimal divergence, with occasional conservative substitutions (L to V and L to I). As viral fusion peptides are known to be highly conserved within a family (26), this gave us confidence to proceed with a comprehensive mutagenesis study of the putative fusion peptide, with fusion ability monitored by a cell-cell fusion assay. We initially took a conservative approach and carried out a replacement of individual amino acids with alanine residues. In all cases, mutations had limited or no effect on S protein assembly and cell surface expression; however, we saw marked effects on the ability to cause cell-cell fusion. In particular the L803A, L804A, and F805A substitutions had major effects on fusion, with fusion of the L804A mutant being undetectable in a highly sensitive luciferase-based fusion assay. Other residues with major effects on fusion (20% or less of wild-type levels) were K807A, D812A, and F815A. Notably, mutation of the new N terminus produced after cleavage at R797 (S798A) had very little effect on cell-cell fusion. To date, mutations to more hydrophilic residues, which may have more dramatic effects on fusion, have not been carried out for most of the residues within the S2 fusion peptide.

To confirm these results in the context of a virus particle, we created MLV pseudovirions containing wild-type and mutant SARS-CoV S proteins. In some cases, particularly for the apparently fusion-critical L803 and L804 residues, alanine sub-

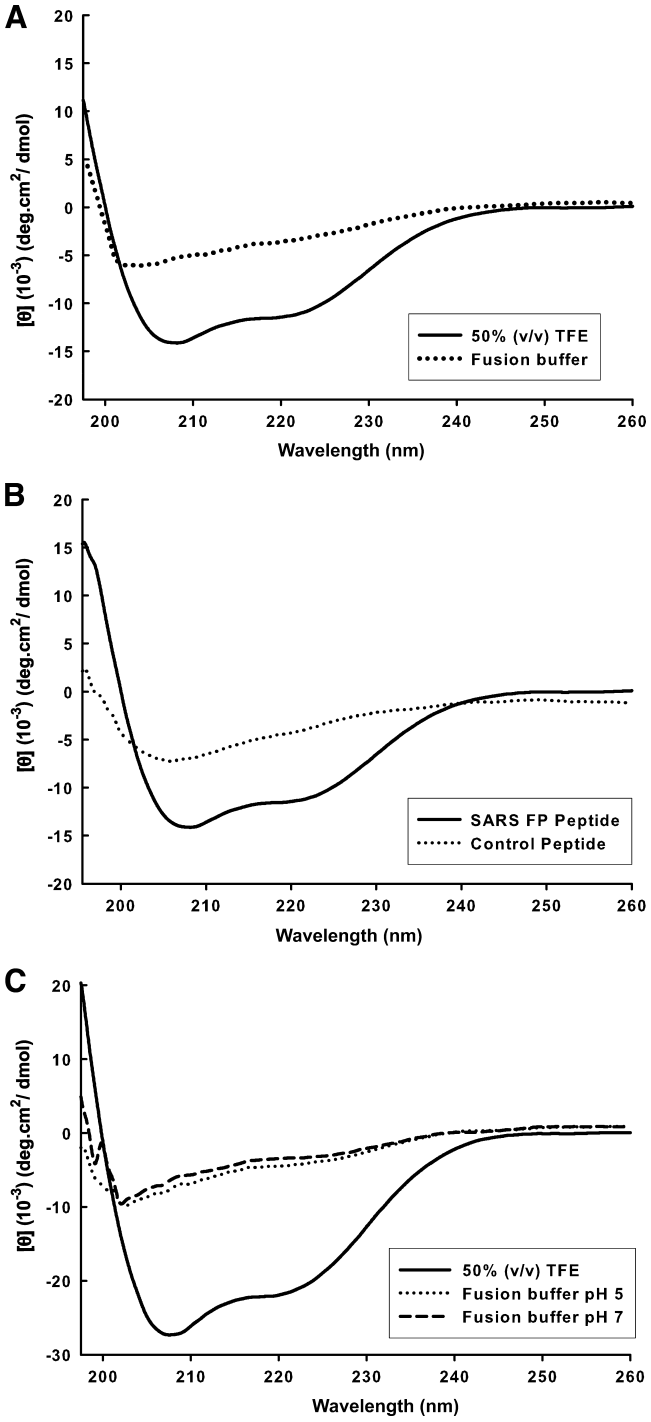


FIG. 9. The proposed SARS-CoV S2 fusion peptide has the propensity to form helical secondary structure. (A) CD spectrum (mean residue ellipticity) of the SARS-CoV S2 fusion peptide (solid line) in a TFE/fusion buffer ratio of 50% (vol/vol) at 37°C or in fusion buffer alone (dotted line). (B) CD spectrum (mean residue ellipticity) of the SARS-CoV S2 fusion peptide (FP; solid line) alongside a control peptide (dotted line) in a TFE/fusion buffer ratio of 50% (vol/vol) at 37°C. (C) CD spectrum (mean residue ellipticity) of the short SARS-CoV S2 fusion peptide (solid line) in a TFE/fusion buffer ratio of 50% (vol/vol) at 37°C or in fusion buffer alone at either pH 5.0 (dotted line) or pH 7.0 (dashed line). deg, degree.

stitutions could not be rescued in pseudovirus particles. In these cases, we made additional substitutions, with the L803E and L803T mutations allowing efficient incorporation. The reasons for the differences in particle incorporation are currently unclear as both L803A and L804A showed nearly normal levels of cell surface expression. Pseudoparticle transduction was determined following both endosomal and nonendosomal routes, and in both cases results were essentially in line with cell-cell fusion data; i.e., fusion-critical residues (<20% of the wild-type level) were L803, L804, and F805, along with D812. The K807 and F815 residues seemed less critical in virus entry assays. Mutations at S798 failed to be incorporated into virus particles, and so the role of this residue could not be determined in this assay. Overall, these experiments appeared to point to L803, L804, and F805 as a fusion-active core of the proposed fusion peptide, with the N-terminal S798 residue being of only limited importance.

To examine the fusion peptide more biochemically, we carried out lipid-mixing and spectroscopy assays. We initially assessed a long version of the peptide (SFIEDLLFNKVTLAD AGF), but due to the apparent importance of the more N-terminal hydrophobic resides (L803, L804, and F805), we also examined a short version of the peptide (SFIEDLLF) in lipid-mixing assays. By spectroscopy, the long and short peptides did not show any intrinsic structure but showed significant α-helical content in the presence of TFE. We were not able to assess the structure in the presence of liposomes due to fusion and aggregation of liposomes when peptide was added. In both cases, lipid-mixing experiments showed that the peptides were fusion active; both peptides were more active at pH 5 than at pH 7.

Notably, L803, L804, and F805 are the initial residues of a major antigenic determinant of SARS-CoV S (Leu 803-Ala 828) that is capable of inducing neutralizing antibodies (40). This SARS-CoV epitope is also homologous to an immunodominant neutralizing domain on the MHV S2 subunit (7). It will be interesting to see if these neutralizing antibodies mediate their effects during membrane fusion, as found for the closely located 5B19 epitope of MHV S (33).

While a crystal structure of the SARS-CoV S ectodomain has not yet been solved, a predictive model of the quaternary structure is available (Protein Data Bank code 1T7G) (3). In the context of this model, the novel S2 fusion peptide is mainly helical (especially the conserved residues SXIEDLLF), with a short central unstructured region, and is in a relatively exposed position midway down the trimeric spike protein complex (Fig. 10). This structure and position within the S trimer are consistent with its function as a viral fusion protein.

In our initial bioinformatics analysis of the predicted SARS-CoV S fusion peptide, we were initially surprised by the presence of several charged residues, i.e., E801, D802, K807, and D812. While fusion peptides from pH-dependent viruses, such influenza virus, often contain negatively charged residues, the presence of positively charged residues is unusual. The three-dimensional structure of the proposed S2 fusion peptide (SFI EDLLFNKVTLADAGF) in this model predicts two short helices separated by a short unstructured region. While there is no obvious proline-containing turn motif (as in ASLV or EBOV), we consider that the SARS-CoV S2 fusion peptide does not follow the N-terminal α-helix pattern of influenza

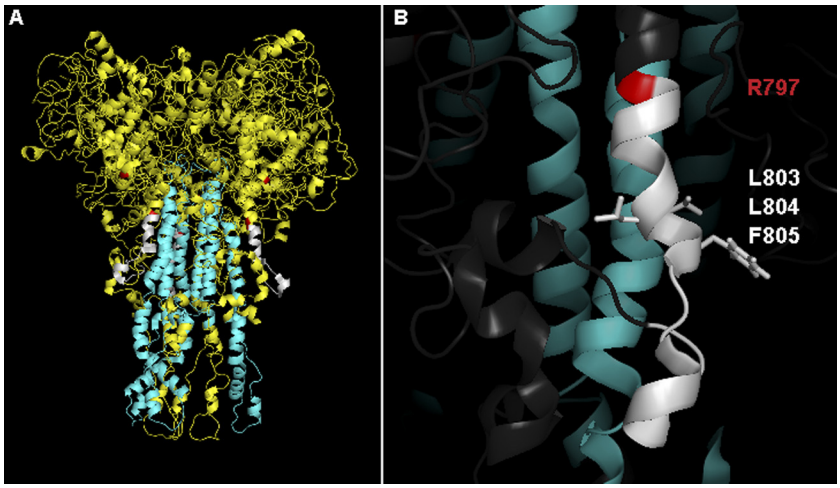


FIG. 10. Structural model of the SARS-CoV S2. (A) A three-dimensional model of the SARS-CoV S protein ectodomain trimer is shown in cartoon form, based on Protein Data Bank file 1T7G. The figure was generated in MacPyMOL (DeLano Scientific), with the proposed fusion peptide shown in white and the S2 cleavage site (R797) shown in magenta. (B) The side chains of the proposed fusion-active core (L803, L804, and F805) are shown in enlarged form.

virus or human immunodeficiency virus type 1 but, rather, comprises an internal fusion peptide more like that of ASLV or Ebola virus, which is exposed by a proximal cleavage event. The major difference for SARS-CoV S would be that the known S2 cleavage site is closer to the core residues of the proposed fusion peptide (6 to 8 amino acids away) rather than the 20 to 30 amino acids found for ASLV or EBOV (24, 27, 35, 38). It is also possible that alternative cleavage sites within the S2 domain could result in exposure of the fusion peptide. In this scenario, the charged residues of the proposed SARS-CoV S fusion peptide (E801, D802, K807, and D812) would lie outside the membrane-penetrating region and would be cytosolic or interact with the phospholipid head groups. In terms of structure, the membrane-penetrating, fusion-active core of the SARS-CoV S2 fusion peptide would comprise residues L803, L804, and F805 and may be composed of a hydrophobic pocket in conjunction with a short $3_{10}$-helix, as proposed for EBOV (10, 24) and for influenza virus at low pH (18), although this will need to be addressed experimentally.

The data presented here suggest the presence of a critical fusion peptide close to the S2 cleavage site; however, in the absence of a crystal structure of SARS-CoV S in both pre- and postfusion forms, as well as more biophysical measurements of peptide intercalation into membranes in the context of the complete S protein, we do not have formal proof that the region SFIEDLLFNKVTLADAGF constitutes the only fusion peptide for SARS-CoV S. It is possible that the fusion peptide identified here functions in conjunction with other fusion peptides or membrane-intercalating regions of the spike protein identified in previous work.

While the low endosomal pH is important for SARS-CoV entry, other nonendosomal entry routes can occur. Thus, it is presently unclear whether low pH is needed only for activation of cathepsins priming the SARS-CoV S protein or whether low pH has a more direct role. Overall, however, it seems likely that CoVs in general can mediate membrane fusion at a range of pH values. The fusion peptide characterized here is highly conserved across the *Coronaviridae*, especially in the core IE DLLF sequence. It seems likely that this sequence, working in conjunction with other membrane-active regions of the spike protein, is an important feature of this diverse virus family at various pH values and with different cleavage events that could result in fusion peptide exposure.

## ACKNOWLEDGMENTS

We thank Ruth Collins, Holger Sondermann, and Brian Crane for their help and advice during the course of this work and Michael Farzan, Tom Gallagher, and Jean Dubuisson for their kind provision of reagents. We also thank A. Damon Ferguson for technical assistance and all members of the Whittaker laboratory for helpful suggestions.

I.G.M. was the recipient of a fellowship from the National Institutes of Health (NIGMS), grant F31 GM082084. S.L.R. was the recipient of a Cornell University Provost's Diversity fellowship. This work was also supported by the Cornell University Nanobiotechnology Center, an STC program of the National Science Foundation under agreement number ECS-987677, and the National Institutes of Health (NIAID), grants R03 AI060946 and R21 AI076258.

## REFERENCES

1. **Bartosch, B., J. Dubuisson, and F. L. Cosset.** 2003. Infectious hepatitis C virus pseudo-particles containing functional E1-E2 envelope protein complexes. J. Exp. Med. **197:**633–642.
2. **Belouzard, S., V. C. Chu, and G. R. Whittaker.** 2009. Activation of the SARS coronavirus spike protein via sequential proteolytic cleavage at two distinct sites. Proc. Natl. Acad. Sci. USA **106:**5871–5876.
3. **Bernini, A., O. Spiga, A. Ciutti, S. Chiellini, L. Bracci, X. Yan, B. Zheng, J. Huang, M. L. He, H. D. Song, P. Hao, G. Zhao, and N. Niccolai.** 2004. Prediction of quaternary assembly of SARS coronavirus peplomer. Biochem. Biophys. Res. Commun. **325:**1210–1214.
4. **Bosch, B. J., and P. J. Rottier.** 2008. Nidovirus Entry into Cells, p. 157–178. *In* S. Perlman, T. Gallagher, and E. J. Snijder (ed.), Nidoviruses. ASM Press, Washington, DC.
5. **Bosch, B. J., R. van der Zee, C. A. de Haan, and P. J. Rottier.** 2003. The coronavirus spike protein is a class I virus fusion protein: structural and functional characterization of the fusion core complex. J. Virol. **77:**8801–8811.
6. **Chambers, P., C. R. Pringle, and A. J. Easton.** 1990. Heptad repeat sequences are located adjacent to hydrophobic regions in several types of virus fusion glycoproteins. J. Gen. Virol. **71:**3075–3080.
7. **Daniel, C., R. Anderson, M. J. Buchmeier, J. O. Fleming, W. J. Spaan, H. Wege, and P. J. Talbot.** 1993. Identification of an immunodominant linear

neutralization domain on the S2 portion of the murine coronavirus spike glycoprotein and evidence that it forms part of complex tridimensional structure. J. Virol. **67:**1185–1194.
8. **Durell, S. R., I. Martin, J. M. Ruysschaert, Y. Shai, and R. Blumenthal.** 1997. What studies of fusion peptides tell us about viral envelope glycoprotein-mediated membrane fusion (review). Mol. Membr. Biol. **14:**97–112.
9. **Earp, L. J., S. E. Delos, H. E. Park, and J. M. White.** 2005. The many mechanisms of viral membrane fusion proteins. Curr. Top. Microbiol. Immunol. **285:**25–66.
10. **Freitas, M. S., L. P. Gaspar, M. Lorenzoni, F. C. Almeida, L. W. Tinoco, M. S. Almeida, L. F. Maia, L. Degreve, A. P. Valente, and J. L. Silva.** 2007. Structure of the Ebola fusion peptide in a membrane-mimetic environment and the interaction with lipid rafts. J. Biol. Chem. **282:**27306–27314.
11. **Gomara, M. J., P. Mora, I. Mingarro, and J. L. Nieva.** 2004. Roles of a conserved proline in the internal fusion peptide of Ebola glycoprotein. FEBS Lett. **569:**261–266.
12. **Goodman, M., I. Listowsky, Y. Masuda, and F. Boardman.** 1963. Conformational aspects of polypeptides. VIII. Helical assignments via far ultraviolet adsorption spectra and optical activity. Biopolymers **1:**33–42.
13. **Guillen, J., R. F. de Almeida, M. Prieto, and J. Villalain.** 2008. Structural and dynamic characterization of the interaction of the putative fusion peptide of the S2 SARS-CoV virus protein with lipid membranes. J. Phys Chem. B **112:**6997–7007.
14. **Guillen, J., P. K. Kinnunen, and J. Villalain.** 2008. Membrane insertion of the three main membranotropic sequences from SARS-CoV S2 glycoprotein. Biochim. Biophys. Acta **1778:**2765–2774.
15. **Guillen, J., M. R. Moreno, A. J. Perez-Berna, A. Bernabeu, and J. Villalain.** 2007. Interaction of a peptide from the pre-transmembrane domain of the severe acute respiratory syndrome coronavirus spike protein with phospholipid membranes. J. Phys Chem. B **111:**13714–13725.
16. **Guillen, J., A. J. Perez-Berna, M. R. Moreno, and J. Villalain.** 2008. A second SARS-CoV S2 glycoprotein internal membrane-active peptide. Biophysical characterization and membrane interaction. Biochemistry **47:**8214–8224.
17. **Guillen, J., A. J. Perez-Berna, M. R. Moreno, and J. Villalain.** 2005. Identification of the membrane-active regions of the severe acute respiratory syndrome coronavirus spike membrane glycoprotein using a 16/18-mer peptide scan: implications for the viral fusion mechanism. J. Virol. **79:**1743–1752.
18. **Han, X., J. H. Bushweller, D. S. Cafiso, and L. K. Tamm.** 2001. Membrane structure and fusion-triggering conformational change of the fusion domain from influenza hemagglutinin. Nat. Struct. Biol. **8:**715–720.
19. **Han, X., and L. K. Tamm.** 2000. A host-guest system to study structure-function relationships of membrane fusion peptides. Proc. Natl. Acad. Sci. USA **97:**13097–13102.
20. **Howard, M. W., E. A. Travanty, S. A. Jeffers, M. K. Smith, S. T. Wennier, L. B. Thackray, and K. V. Holmes.** 2008. Aromatic amino acids in the juxtamembrane domain of severe acute respiratory syndrome coronavirus spike glycoprotein are important for receptor-dependent virus entry and cell-cell fusion. J. Virol. **82:**2883–2894.
21. **Klenk, H. D., and W. Garten.** 1994. Host cell proteases controlling virus pathogenicity. Trends Microbiol. **2:**39–43.
22. **Lague, P., B. Roux, and R. W. Pastor.** 2005. Molecular dynamics simulations of the influenza hemagglutinin fusion peptide in micelles and bilayers: conformational analysis of peptide and lipids. J. Mol. Biol. **354:**1129–1141.
23. **Lai, A. L., Y. Li, and L. K. Tamm.** 2005. Interplay of proteins and lipids in virus entry by membrane fusion, p. 279–303. *In* L. K. Tamm (ed.), Protein-lipid interactions. Wiley-VCH Verlag GmbH, Weinheim, Germany.
24. **Lee, J. E., M. L. Fusco, A. J. Hessell, W. B. Oswald, D. R. Burton, and E. O. Saphire.** 2008. Structure of the Ebola virus glycoprotein bound to an antibody from a human survivor. Nature **454:**177–182.
25. **Lu, Y., T. L. Neo, D. X. Liu, and J. P. Tam.** 2008. Importance of SARS-CoV spike protein Trp-rich region in viral infectivity. Biochem. Biophys. Res. Commun. **371:**356–360.
26. **Martin, I., and J. M. Ruysschaert.** 2000. Common properties of fusion peptides from diverse systems. Biosci. Rep. **20:**483–500.
27. **Perez, L. G., and E. Hunter.** 1987. Mutations within the proteolytic cleavage site of the Rous sarcoma virus glycoprotein that block processing to gp85 and gp37. J. Virol. **61:**1609–1614.
28. **Petit, C. M., J. M. Melancon, V. N. Chouljenko, R. Colgrove, M. Farzan, D. M. Knipe, and K. G. Kousoulas.** 2005. Genetic analysis of the SARS-coronavirus spike glycoprotein functional domains involved in cell-surface expression and cell-to-cell fusion. Virology **341:**215–230.
29. **Sainz, B., Jr., J. M. Rausch, W. R. Gallaher, R. F. Garry, and W. C. Wimley.** 2005. Identification and characterization of the putative fusion peptide of the severe acute respiratory syndrome-associated coronavirus spike protein. J. Virol. **79:**7195–7206.
30. **Sainz, B., Jr., J. M. Rausch, W. R. Gallaher, R. F. Garry, and W. C. Wimley.** 2005. The aromatic domain of the coronavirus class I viral fusion protein induces membrane permeabilization: putative role during viral entry. Biochemistry **44:**947–958.
31. **Song, H. C., M. Y. Seo, K. Stadler, B. J. Yoo, Q. L. Choo, S. R. Coates, Y. Uematsu, T. Harada, C. E. Greer, J. M. Polo, P. Pileri, M. Eickmann, R. Rappuoli, S. Abrignani, M. Houghton, and J. H. Han.** 2004. Synthesis and characterization of a native, oligomeric form of recombinant severe acute respiratory syndrome coronavirus spike glycoprotein. J. Virol. **78:**10328–10335.
32. **Struck, D. K., D. Hoekstra, and R. E. Pagano.** 1981. Use of resonance energy transfer to monitor membrane fusion. Biochemistry **20:**4093–4099.
33. **Taguchi, F., and Y. K. Shimazaki.** 2000. Functional analysis of an epitope in the S2 subunit of the murine coronavirus spike protein: involvement in fusion activity. J. Gen. Virol. **81:**2867–2871.
34. **Tamm, L. K., and X. Han.** 2000. Viral fusion peptides: a tool set to disrupt and connect biological membranes. Biosci. Rep. **20:**501–518.
35. **Volchkov, V. E., H. Feldmann, V. A. Volchkova, and H. D. Klenk.** 1998. Processing of the Ebola virus glycoprotein by the proprotein convertase furin. Proc. Natl. Acad. Sci. USA **95:**5762–5767.
36. **Watanabe, R., S. Matsuyama, K. Shirato, M. Maejima, S. Fukushi, S. Morikawa, and F. Taguchi.** 2008. Entry from cell surface of SARS coronavirus with cleaved S protein as revealed by pseudotype virus bearing cleaved S protein. J. Virol. **82:**11985–11991.
37. **Wentworth, D. E., and K. V. Holmes.** 2007. Coronavirus binding and entry, p. 3–31. *In* V. Thiel (ed.), Coronaviruses: molecular and cellular biology. Caister Academic Press, Norfolk, United Kingdom.
38. **White, J. M., S. E. Delos, M. Brecher, and K. Schornberg.** 2008. Structures and mechanisms of viral membrane fusion proteins: multiple variations on a common theme. Crit. Rev. Biochem. Mol. Biol. **43:**189–219.
39. **Xiao, X., S. Chakraborti, A. S. Dimitrov, K. Gramatikoff, and D. S. Dimitrov.** 2003. The SARS-CoV S glycoprotein: expression and functional characterization. Biochem. Biophys. Res. Commun. **312:**1159–1164.
40. **Zhang, H., G. Wang, J. Li, Y. Nie, X. Shi, G. Lian, W. Wang, X. Yin, Y. Zhao, X. Qu, M. Ding, and H. Deng.** 2004. Identification of an antigenic determinant on the S2 domain of the severe acute respiratory syndrome coronavirus spike glycoprotein capable of inducing neutralizing antibodies. J. Virol. **78:**6938–6945.